Reference to published article:
Cruz-Hernández, P., Carrero, S., Pérez-López, R., Fernandez-Martinez, A., Lindsay, M.B.J., Dejoie, C., & Nieto, J.M. (2019). Influence of As(V) on precipitation and transformation of schwertmannite in acid mine drainage-impacted waters. *European Journal of Mineralogy (Stuttgart),* 31(2): 237–245. https://doi.org/10.1127/ejm/2019/0031-2821

Influence of As(V) on precipitation and transformation of schwertmannite in acid mine drainage-impacted waters

Pablo Cruz-Hernández[a,b,*], Sergio Carrero[c], Rafael Pérez-López[a,d], Alejandro Fernandez-Martinez[e], Matthew B.J. Lindsay[f], Catherine Dejoie[g] and José M. Nieto[a,c]

[a] *Department of Earth Sciences, University of Huelva, Huelva 21071, Spain*
[b] *Department of Mining Engineering, University of Chile, FCFM, Santiago, Chile*
[c] *Department of Earth and Planetary Science, University of California Berkeley, Berkeley, 94720, CA, USA*
[d] *Research Center on Natural Resources, Health and the Environment (RENSMA), University of Huelva, Huelva 21071, Spain*
[e] *Univ. Grenoble Alpes, Univ. Savoie Mont-Blanc, CNRS, IRD, IFSTTAR, ISTerre, 38000 Grenoble, France*
[f] *Department of Geological Sciences, University of Saskatchewan, Saskatoon, SK S7N 5E2, Canada*
[g] *European Synchrotron Radiation Facility, 38043 Grenoble, France*

* Corresponding author:
E-mail address: pablo.cruzhdz@gmail.com (P.Cruz-Hernández)

Keywords: schwertmannite; goethite; hematite; ageing; kinetics; acid drainage; arsenic

ABSTRACT

Iron-rich sediments commonly cover riverbeds affected by acid mine drainage (AMD). Initial precipitates are often dominated by schwertmannite, which has an exceptionally high capacity to sequester As and other toxic elements. This poorly crystalline Fe oxyhydroxysulfate rapidly recrystallizes to goethite; however, the influence of trace elements on ageing rates and products is poorly understood. This study examined the influence of As(V) concentrations on the kinetics of schwertmannite precipitation and transformation. Schwertmannite was synthesized in the presence of various initial dissolved As concentrations (*i.e.*, 0–2 mM) and subsequently aged at 40, 60 or 85 °C for 1 h to 300 d. The initial As concentration had a profound impact on schwertmannite precipitation and transformation. Schwertmannite precipitation was inhibited at higher initial As concentrations in favor of pseudo-amorphous Fe-hydroxyarsenate formation. Schwertmannite transformation to goethite was accompanied by sulfate release and, over longer time, As release. Pair distribution function (PDF) analysis of high-energy X-ray diffraction (HEXD) patterns revealed that increasing initial As concentration produced structural defects in associated precipitates. Schwertmannite precipitation exerts an important control on As mobility in AMD-impacted waters; however, this study has demonstrated that the long-term stability of schwertmannite and associated precipitates should be considered when designing AMD remediation strategies and AMD treatment systems.

1. Introduction

Arsenic is considered one of the most hazardous elements for the environment and human health (Mandal & Suzuki, 2002). This metalloid is commonly associated to pyrite (FeS_2) and other minerals including arsenopyrite (FeAsS) in metallic sulfide orebodies. Oxidative weathering of these and other sulfide minerals can acidify water and release high concentrations of sulfate and metal(oid)s including Fe, As, Cd, Cu, Zn, and Pb (Parviainen *et al.*, 2012; Lindsay *et al.*, 2015). Leachate resulting from the oxidation of sulfide-rich wastes derived from mining activities is known as acid mine drainage (AMD) (Nordstrom & Alpers, 1999; Nieto *et al.*, 2013).

Precipitation of poorly crystalline Fe phases occurs under acidic conditions in the presence of high Fe and SO_4 concentrations. These phases include oxy-hydroxides and oxy-hydroxysulfates, such as ferrihydrite ($Fe_{10}O_{14}(OH)_2 \cdot nH_2O$) and schwertmannite ($Fe_8O_8(OH)_x(SO_4)_y \cdot nH_2O$; $x = 8–2y$, $1 < y < 1.75$), (Bigham *et al.*, 1990; Yu *et al.*, 1999; Fernandez-Martinez *et al.*, 2010). Schwertmannite commonly accumulates on AMD-impacted riverbeds, forming sedimentary terrace-like structures (Essalhi *et al.*, 2011; Cruz-Hernández *et al.*, 2016). This oxy-hydroxysulfate phase is an effective scavenger of trace elements, particularly oxyanions, including As (Fukushi *et al.*, 2003a; Regenspurg & Peiffer, 2005; Burton *et al.*, 2009; Adra *et al.*, 2013; Carrero *et al.*, 2015) through pH-dependent adsorption (Schwertmann & Fitzpatrick, 1992; Regenspurg & Peiffer, 2005; Acero *et al.*, 2006; Burton *et al.*, 2009; Maillot *et al.*, 2013) or co-precipitation (Park *et al.*, 2016). However, under natural conditions, schwertmannite transformation to goethite (FeOOH) occurs over weeks (Acero *et al.*, 2006), while transformation to hematite occurs over centuries (Pérez-López *et al.*, 2011; Parviainen *et al.*, 2015) or under hydrothermal conditions (Barham, 1997; Davidson *et al.*, 2008). In spite of the

large number of studies on the subject, the fate of As during transformation remains poorly constrained. Acero *et al.* (2006) suggested that As remains associated with the goethite surface, while other studies have suggested that the transformation to hematite promotes desorption due to decreasing surface site density (Pérez-López *et al.*, 2011; Cruz-Hernández *et al.*, 2016). Bolanz *et al.* (2013) proposed an epitactic intergrowth of angelelite ($Fe_4(AsO_4)O_3$) with hematite, which would retain the majority of As derived from the initial poorly crystalline phases.

This study examined schwertmannite precipitation and transformation in the presence of increasing initial dissolved As(V) concentrations. The main aim was to quantify differences in the kinetics of schwertmannite precipitation and transformation, and to discern the final fate of As during ageing of the precipitates. In addition, structural defects associated with As incorporation were characterized using pair distribution function (PDF). This technique has been successfully implemented on structural studies in poorly crystalline phases (Fernandez-Martinez *et al.*, 2010; Wang *et al.*, 2015). Furthermore, PDF analysis has also helped to describe the structure of adsorbates on similar phases (Harrington *et al.*, 2010; Li *et al.*, 2011). The precursor phase, schwertmannite, was synthesized based on previous protocols (Loan *et al.*, 2004; Eskandarpour *et al.*, 2008) in the presence of different As(V) concentrations at 85, 60 and 40 °C during different time periods. These experiments are relevant to AMD since they would allow obtaining information on the mineralogical transformations occurring in iron-rich sediments from AMD-affected rivers and assess their influence on As mobility during two similar processes but over different time scales: (1) ageing processes of loose precipitates of schwertmannite in current riverbeds, and (2) diagenetic processes occurring during the sediment maturation. This study contributes important new information that will help optimize the

environmental management of mining wastes. More specifically, new information on kinetics of schwertmannite precipitation and transformation will help improve predictions of long-term contaminant behavior in AMD-impacted waters.

2. Materials and methods

2.1 Sample synthesis

Batch experiments were conducted to evaluate the impact of initial dissolved As(V) concentration on mineralogical changes taking place during schwertmannite precipitation and transformation. Schwertmannite was synthetized by adding previously dehydrated $Fe_2(SO_4)_3 \cdot xH_2O$ in acid-washed 0.5 L polyethylene bottles with double-sealing plugs following the method proposed by Loan *et al.* (2004) and Eskandarpour *et al.* (2008). Both precipitation and transformation of schwertmannite were studied in the presence of different dissolved As(V) concentrations and heat to accelerate the transformation process. Three sets of ageing experiments were carried out as a function of temperature: (1) at 40 °C to determine schwertmannite precipitation rates, (2) at 60 °C to study the transformation of schwertmannite to goethite; and (3) at 85 °C to elucidate possible As adsorption or desorption processes during goethite recrystallization. In each set of experiments, deionized (DI) water was preheated in a calibrated oven for 24 h to the desired temperature (*i.e.*, 40 °C, 60 °C or 85 °C).

Seven initial As(V) concentrations (0, 0.05, 0.125, 0.25, 0.5, 1 and 2 mM) were used by adding different amounts of $Na_2HAsO_4 \cdot 7H_2O$. Given that schwertmannite precipitation occurs spontaneously during the heating of the $Fe_2(SO_4)_3$ solution (pH $\simeq$ 2.1 $\pm$ 0.15), $Na_2HAsO_4 \cdot 7H_2O$ was firstly added to the preheated DI water before precipitation. The solutions remained in the oven for variable time periods, ranging from 1 h to 300 days. After experiments, solutions were

immediately filtered through 0.45 μm nylon syringe filters, acidified with *supra*-pure HNO_3 and stored at 4 °C until analysis. The pH, redox potential (Eh), electric conductivity (EC) and temperature were measured immediately with a portable multi-parameter Crison Mm40+ instrument, calibrated with certified pH buffers (4.01, 7 and 9.2), and with standard solutions for Eh (220 and 468 mV) and conductivity (142 and 1471 μS cm^{-1} and 12.8 mS cm^{-1}). Measured redox electrode potentials were corrected to obtain the Eh with respect to the standard hydrogen electrode (Nordstrom & Wilde, 1998). Solid samples were recovered after each experiment by vacuum filtration through 0.45 μm cellulose nitrate membrane filters. Retained solids were rinsed twice with DI water and dried in a desiccator at room temperature to avoid further mineral transformation.

Schwertmannite, goethite and hematite standards were synthetized without As. Schwertmannite synthesis was performed following the same methodology used for the ageing experiments. Goethite was synthetized by mixing 180 mL of 5 M KOH and 100 mL of 1 M $Fe(NO_3)_2$ diluted to 2 L with DI water (Schwertmann & Cornell, 1991). The solution was heated at 70 °C for 60 h and precipitates were recovered and rinsed three times with DI water. Standards of hematite were synthetized preheating 2 L of 2 mM HNO_3 prepared with DI water to 98 °C, adding 16.06 g of $Fe(NO_3)_2 \cdot 9H_2O$, and ageing at 98 °C for 7 days (Schwertmann & Cornell, 1991). The resulting suspension was collected and rinsed with DI water. All solids were dried in a desiccator at room temperature.

2.2 Analytical methods

Dissolved As, Fe, S, and Na concentrations were determined by inductively coupled plasma-atomic emission spectrometry (ICP-AES; Jobin-Ybon Ultima2). Since the experiment was completely run under oxidizing conditions, the concentration of sulfates was considered as total

S. Dissolved sulfate concentrations were calculated from the total S concentrations, assuming that the presence of other sulfide species was negligible. Analytical error was determined to be <5% and detection limits were: 0.10 mg/L for Fe, 0.08 mg/L for S, 0.02 mg/L for Na and 0.01 mg/L for As. To assess analytical accuracy, the analysis sequence consisted of laboratory standards, quality control solutions analyzed as blind samples, blanks and duplicates. Bulk powder X-ray diffraction (XRD) was performed using a Bruker D8 advance diffractometer with Cu *K*α radiation. The diffractometer was operated at 40 kV and 30 mA, with a 2–65° 2θ scan range, 0.05° 2θ step size, and 20 s acquisition time per step. Further analyses were performed using a JEOL JEM-1011 transmission electron microscope (TEM) fitted with a MEGAVIEW III high-resolution camera. Samples for TEM analysis were suspended in acetone by ultrasonic vibration and an aliquot was dropped on a 2 mm carbon support film grid. The accelerating voltage was fixed at 100 kV during TEM analysis. The ICP-AES, XRD and TEM analyses were performed in the laboratories of the University of Huelva.

High-energy X-ray diffraction (HEXD) measurements were conducted on beamline ID22 at the European Synchrotron Radiation Facility (ESRF, Grenoble, France). Solids obtained from the 0.125 mM $[As]_0$ batches after 8 h, 10 d and 300 d and 40 °C, 60 °C and 85 °C, plus the synthesized schwertmannite, goethite and hematite standards, were powdered and transferred into polyimide (Kapton) capillary tubes. Analysis was performed at room temperature over a *Q*-range of 1–25 $Å^{-1}$. The incident monochromatic X-ray beam had an energy of 70.05 keV (λ = 0.177 Å) and 2-D diffraction patterns were collected in transmission mode using a Perkin Elmer XRD 1621 amorphous-Si flat panel detector. The detector geometry was calibrated using a CeO_2 standard (NIST 679b) and sample patterns were integrated using pyFAI (Kieffer & Karkoulis, 2013). Integrated patterns were corrected for background, Compton scattering and

converted to structure factor, S(Q), using PDFgetX3 (Juhás *et al.*, 2013). The PDF, is related to the structure factor by a Fourier transform,

$$G(r)=2/\pi\int_0^{\infty} Q[S(Q)-1]\sin(Qr)dQ, \quad (1)$$

where $G(r)$ is the PDF, and Q is the scattering vector [$Q = 4\pi\sin(\theta)/\lambda$]. More details on PDF analysis and data corrections can be found in Takeshi & Billinge (2012). Additionally, differential pair distribution function (d-PDF) were obtained by subtracting the PDF of reference samples (As-free Fe-precipitate in concentration sequence) from the PDFs of samples with different $[As]_0$ concentration. Quantitative phase analysis was also performed with linear combination fits of the PDFs, using PDF of reference systems (schwertmannite, goethite and hematite), with the PDFgui software (Farrow *et al.*, 2009).

3. Results and discussion

3.1 Mineralogical composition

Powder Cu *K*α and synchrotron XRD data showed that schwertmannite was the only initial precipitate present in most experiments (Fig. 1a). However, in experiments with the highest As concentrations (*i.e.*, 1 mM at 40 °C; 1 mM at 60 °C; 1 and 2 mM at 85 °C), a poorly crystalline phase other than schwertmannite was detected (Fig. 1b). These diffraction analyses also revealed that schwertmannite transformed into goethite, which progressively appeared in all ageing experiments (Fig. 1c). TEM observations revealed that synthetic schwertmannite aggregates measured 300 nm–1 μm in diameter and exhibited pin-cushion morphology (Fig. 1a). These aggregates were comprised of needle-like nanocrystals measuring 5 nm in diameter and 30 nm long. Goethite crystals were elongated (between 300 nm and 1 μm and 10 and 25 nm) (Fig. 1c). The poorly crystalline phase precipitated from high $[As]_0$ solutions (*i.e.*, ≥1 mM As) exhibited

high As (25 ± 5 wt%), Fe (≈33 ± 2 wt%) and O (≈38 ± 10 wt%) contents plus minor S (<4 wt%). The TEM images revealed that this phase formed granular aggregates 10–50 nm in diameter (Fig. 1b), while the HEXD pattern exhibited two broad diffraction peaks at 0.30 and 0.16 nm (Fig. 1b). These peaks correspond to an amorphous Fe-hydroxyarsenate (FeOHAs), which precipitates preferentially to schwertmannite at dissolved molar As/Fe ratios greater than 0.15 (Krause & Ettel, 1989; Carlson *et al.*, 2002). Paktunc *et al.* (2008) described this phase as an amorphous precursor of scorodite ($FeAsO_4 \cdot 2H_2O$). Overall, these findings are consistent with previous studies showing that dissolved As concentration decrease the crystallinity of initial precipitates.

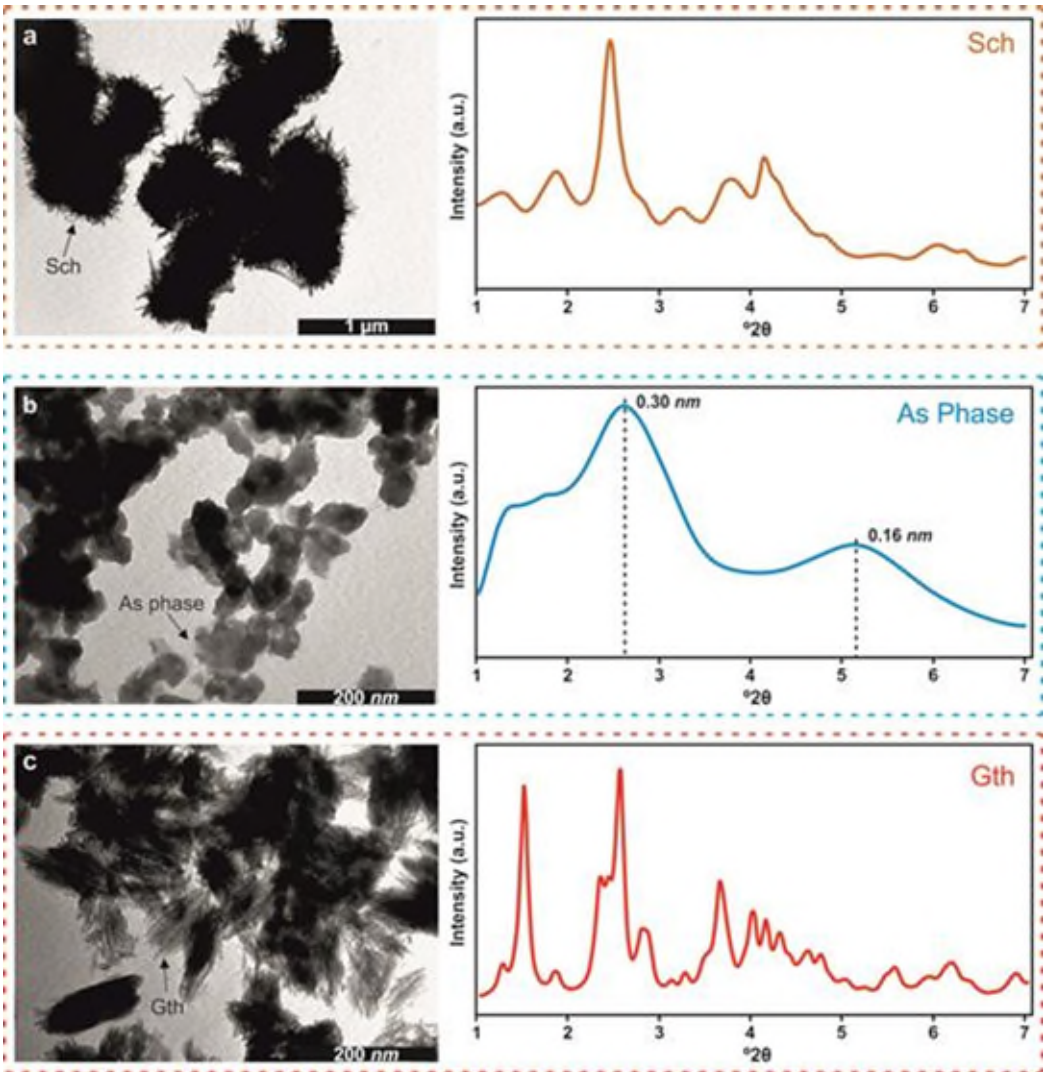

Figure 1. TEM pictures and HEXD patterns of (a) schwertmannite from an experiment at 60 °C with no $[As]_0$ during 2 h; (b) pseudo-amorphous FeOHAs from an experiment performed at 40 °C with $[As]_0$ = 1 mM during 48 h; (c) goethite obtained in an experiment at 85 °C during 150 days with no $[As]_0$.

3.2 Chemical evolution

Transformation of initial precipitates produced distinct changes in physico-chemical parameters, which are characteristic of precipitation and transformation processes (Tables I, II and III, and Figures I, II and III from Supplementary Material linked to this article and freely available at https://pubs-geoscienceworld-org.cyber.usask.ca/eurjmin). The decrease of pH over time was indicative of schwertmannite transformation to goethite, which releases H^+ and

acidifies associated waters (Bigham *et al.*, 1996; Gagliano *et al.*, 2004). In addition, goethite is stable in acid environments such as pH ≈ 2, but it requires lower Eh (Bigham *et al.*, 1996; Caraballo *et al.*, 2013).

Dissolved $[Fe]_T$ and $[SO_4]_T$ concentrations broadly exhibited similar behavior in all experiments conducted at the same temperature (Fig. 2). At the onset of the experiments, dissolved Fe and SO_4 concentrations decreased during initial precipitation reactions. However, $[SO_4]_T$ reached a minimum concentration and subsequently increased again to within 10% of the initial dissolved concentration. In contrast, $[Fe]_T$ reached steady-state after the initial decrease and was at or near detection limit for the rest of the experiments. Trends in $[As]_T$ at the onset of the experiment were concomitant with $[SO_4]_T$ and $[Fe]_T$; however, long-term $[As]_T$ trends were similar to $[SO_4]$, which increased toward the end of the experiments (Fig. 3).

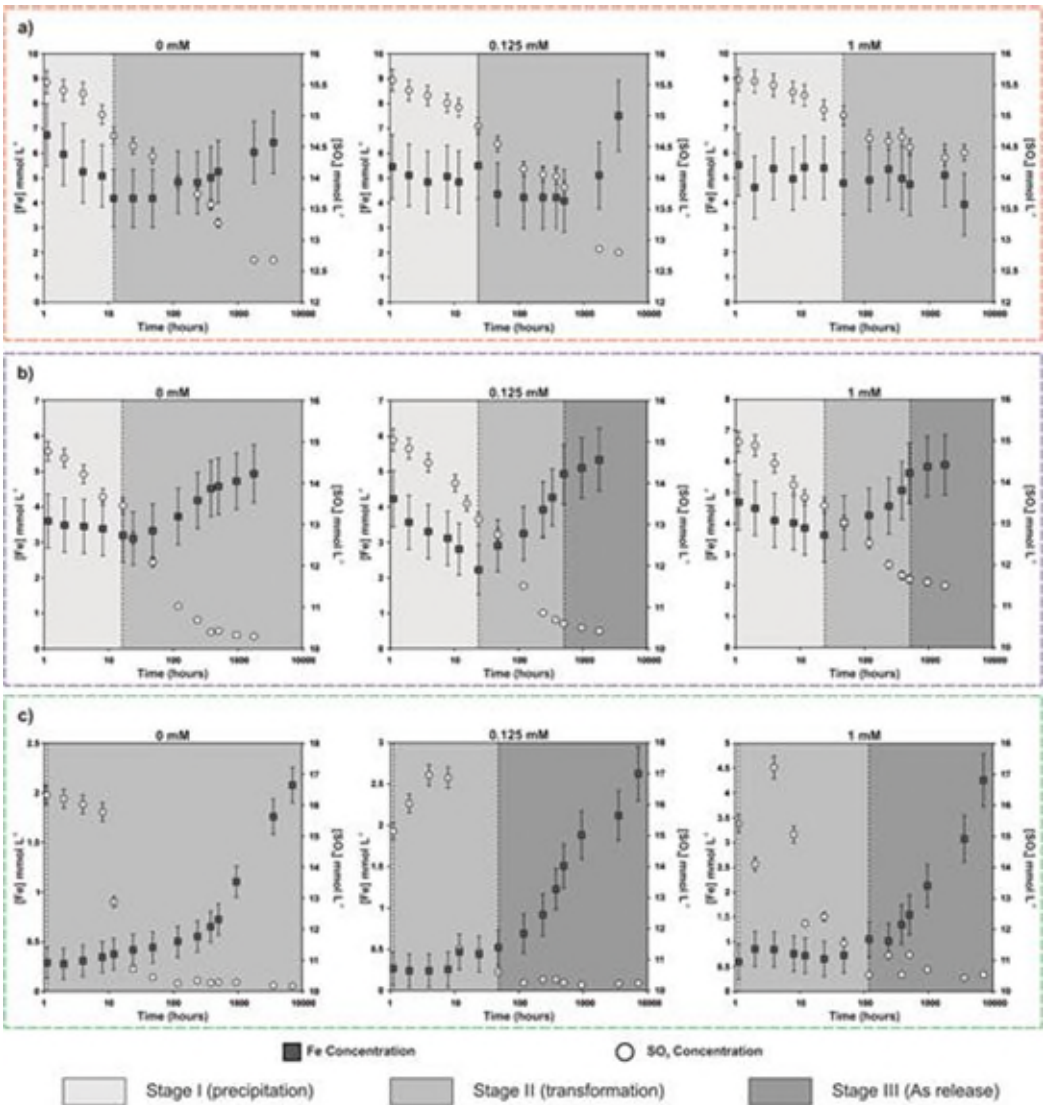

Figure 2. [Fe] (□) and [SO4] (○) concentration of supernatant water at (a) 40 °C, (b) 60 °C and (c) 85 °C. Full chemical information is included as Supplementary Material.

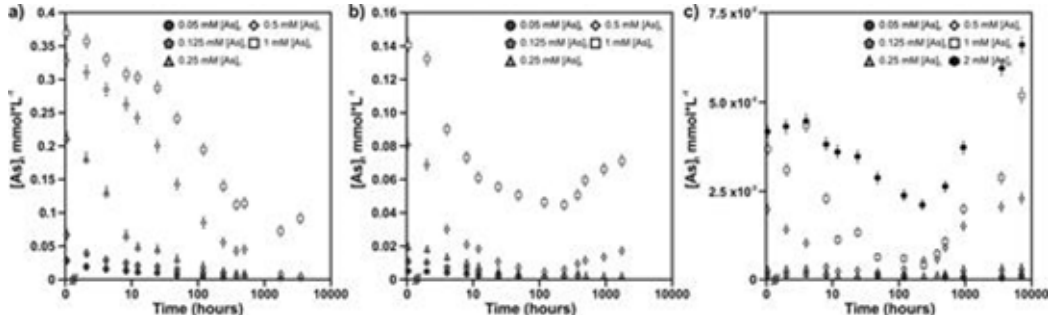

Figure 3. [As] concentration of supernatant water at (a) 40 °C, (b) 60 °C and (c) 85 °C.

Three different reaction stages were defined based on the chemical and mineralogical trends observed during the experiments: (Stage I) initial decrease in $[Fe]_T$ and $[SO_4]_T$ during nucleation and precipitation of the precursor Fe phase (*i.e.*, schwertmannite) except when $[As]_0$ was ≥1 mM; (Stage II) following the initial $[Fe]_T$ and $[SO_4]_T$ decreases, $[SO_4]_T$ began to increase while $[Fe]_T$ continued to decline during the transformation of schwertmannite into goethite; and (Stage III) solution-goethite equilibrium was indicated by steady-state $[Fe]_T$ and $[As]_T$ increase due to desorption into solution. This As release produced concentration up to 10% of $[As]_0$ (Fig. 3); however, unlike Fe, $[As]_T$ did not reach a steady-state and progressively increased over the course of the experiment (Fig. 4). Therefore, As concentration may continue to increase over a longer time.

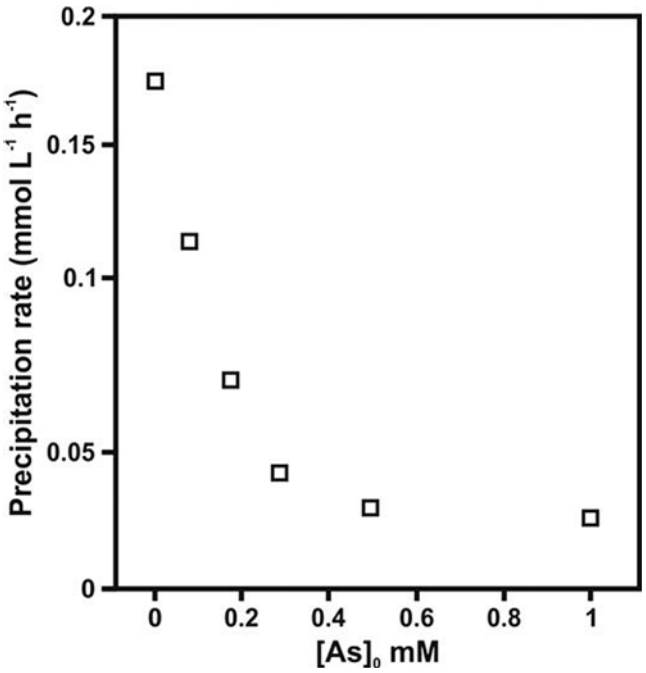

Figure 4. Calculated precipitation rates at 0, 0.05, 0.125, 0.25, 0.5 and 1 mM $[As]_0$.

The main difference between the sets of ageing experiments (40, 60 and 85 °C) is the duration of these three stages. Stage I was much longer in the 40 °C experiments (*i.e.*, between 10 and 100 h) compared to the higher temperatures. The continuous decrease in $[Fe]_T$ to steady-state

observed at 40 °C can be used to calculate precipitation rates of Fe phases. In contrast, observed $[SO_4]_T$ variations among experiments were dependent on $[As]_0$ and, at high $[As]_0$ values (*i.e.*, ≥1 mM), transformation to goethite was inhibited. For the 60 °C experiments, nucleation and precipitation (Stage I) of schwertmannite or Fe-hydroxyarsenate was complete within 1 h of initiating the experiment. At this temperature, the minimum $[SO_4]_T$ was reached between 24 and 48 h and the subsequent progressive release of SO_4 during transformation (Stage II) to goethite was clearly defined. Arsenic release during transformation was observed in the 60 °C experiments containing high $[As]_0$ (*i.e.*, 0.5 and 1 mM); however, the increase in $[As]_T$ was more pronounced in the 85 °C experiments. For the 85 °C experiments, nucleation and precipitation (Stage I) was complete and transformation (Stage II) had started within the first hour. During Stage II of this experiment, $[SO_4]_T$ gradually increased from the minimum reached during Stage I until reaching the initial concentration used to synthesize schwertmannite. Despite this SO_4 release, $[Fe]_T$ decreased by 78% after between 12 and 48 h and remained low for the remaining of the experiments. In the experiments at 85 °C, the Stage III corresponding to the release of As to solution is better seen.

3.3 Precipitation and transformation rates

In the 40 °C ageing experiments, the initial precipitation (Stage I) of the precursor Fe phase is well-defined. Hence, it is possible to calculate the precipitation rates (mmol L^{-1} h^{-1}) by linear regression where the change in [Fe] is linear with time. In the As-free experiment, the precipitation rate of schwertmannite over the pH range 2–2.5 was 0.19 mmol Fe L^{-1} h^{-1}. Furthermore, schwertmannite precipitation rates decreased with increasing $[As]_0$ (0.11, 0.04, 0.036 and 0.032 mmol Fe L^{-1} h^{-1} in experiments where $[As]_0$ = 0.05, 0.125, 0.25, 0.5, and 1 mM). Note that the precursor phase for experiments at 1 mM $[As]_0$ is a Fe-hydroxyarsenate

instead of schwertmannite; however, the precipitation rate calculated from $[Fe]_T$ followed the same general trend. Correlating these precipitation rates with $[As]_0$ revealed that the precipitation of schwertmannite is slowed as $[As]_0$ increases (Fig. 4). Although the Stage I is less well defined in the experiments at 60 °C, the calculation of precipitation rates during the first hour and their correlation with $[As]_0$ are fully consistent with the observations found in the experiments at 40 °C (Fig. IV in Supplementary Material).

The influence of the $[As]_0$ on the transformation rates of the precursor Fe phase into goethite was observed from the determination of the goethite proportion in the samples by linear combination fitting of the PDF analysis in the experimental sets where the stage II was better-defined, at 60 °C and 85 °C. Figure 5 shows goethite content in the samples (wt%) *vs.* $[As]_0$. In the case of the experiments at 60 °C, the time-lapse chosen was 10 days (Fig. 5a), while at 85 °C the samples were left during 300 days (Fig. 5b). The findings indicate that the proportion of goethite and, hence, the transformation rate of schwertmannite also decreases with the increase of $[As]_0$ in solution. Thus, the transformation rate of schwertmannite to goethite is also drastically decelerated.

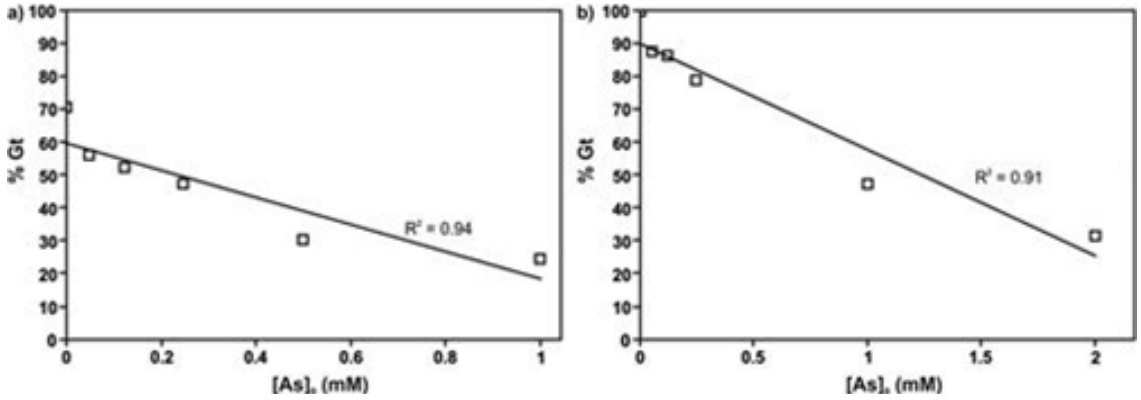

Figure 5. Goethite content of solid samples (wt%) compared to $[As]_0$ experiments at (a) 60 °C aged during 10 days, and (b) 85 °C aged during 300 days.

3.4 Structural implications

The incorporation of As to the structure of Fe-precipitates has several consequences. Previous studies suggest that S and As – as SO_4 and AsO_4, respectively – share a position in the structure of schwertmannite (Burton *et al.*, 2009; Antelo *et al.*, 2012). Figure 6a shows PDF analyses of precipitates collected after 10 days from all experiments (*i.e.*, $[As]_0$ = 0, 0.05, 0.125, 0.25, 0.5 and 1 mM) conducted at 60 °C. In addition, d-PDF shows the short-range order (<4 Å) around As in the solid phases (Fig. 6b). This set of samples was selected as an example, but identical results were obtained for other sets of experiments (Fig. V in Supplementary Information). PDF results revealed that the increase in $[As]_0$ yields precipitates with similar structural features, but lower crystallinity and shorter coherent domain based on the decreasing intensity and widening of the peaks, especially in long-range pairs (Fig. 6a).

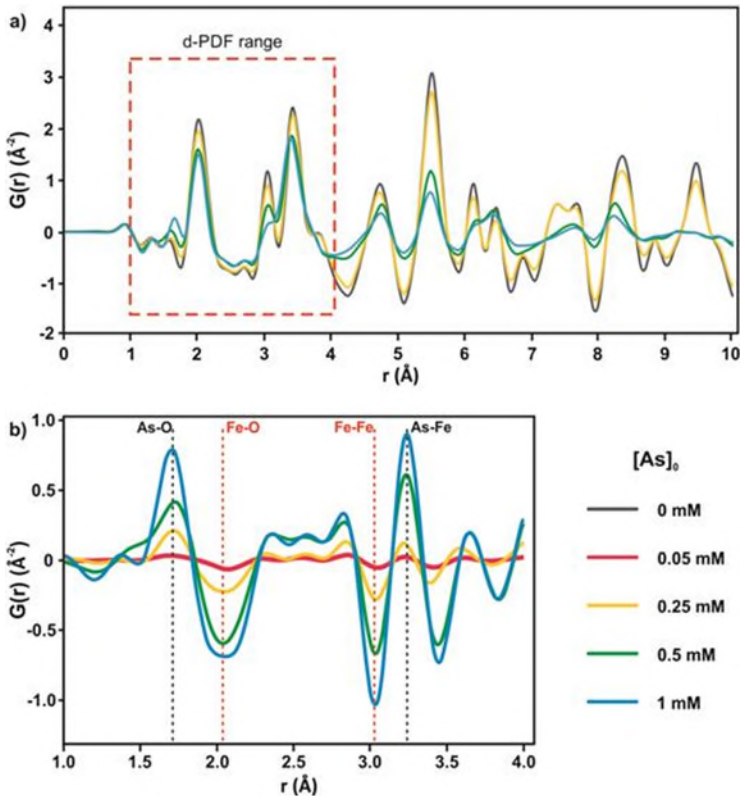

Figure 6. (a) PDF analysis and (b) d-PDF of As in samples aged during 10 days at 60 °C and loaded with different $[As]_0$.

The d-PDF (Fig. 6b) indicates that arsenate is located as bidentate binucleate inner-sphere position. This coordination is congruent with the presence of two positive peaks at ~1.68 and ~3.3 Å, related to As–O distance in an undistorted arsenate tetrahedron and As–Fe distance, respectively, where arsenate tetrahedra form two covalent bonds with the Fe-framework (Harrington *et al.*, 2010). In addition, two negative peaks at ~1.98 Å and ~3.0 Å, which correspond to Fe–O (first neighbor) and O–O bonds in the Fe-framework are reduced or distorted. Thus, As incorporation provokes vacancies of Fe octahedra or important deformations. The accumulation of these defects avoids the development of further periodicity in samples with high As load, reducing the coherent domain and, therefore, the crystallinity of the phase.

Ageing also reduces the incorporation of As in the structure, inasmuch as the As–O peak (~1.68 Å) is slightly less intense in experiments performed at higher temperatures, although the effect of As concentration in the structure is similar in all isothermal experiments. Arsenic inhibits the fixation of sulfates in the structure, likely due to the fact that both share the same position (Burton *et al.*, 2013; Wang *et al.,* 2015) and to the high affinity of As with these precipitates (Fukushi *et al.*, 2003b).

4. Conclusion

This study examined the effects of As(V) on schwertmannite precipitation, on schwertmannite transformation into goethite, and on subsequent goethite re-crystallization. In addition, kinetics of precipitation and transformation have been calculated at short, medium and long term with different concentrations of As(V). Arsenic controls the nucleation, precipitation and transformation processes of the phases, but also is released from their structures once these become more crystalline. In addition, using the d-PDF it has been possible to detect the structural implications of introducing As into schwertmannite, even forming a new amorphous phase at

high $[As]_0$. The high affinity of schwertmannite for other elements such as As controls their mobility at short time-scales, increasing the natural attenuation of pollutants in AMD systems. However, the poor stability of this phase transforms an initial solution into a future source of contamination in long time-scale terms, as it has been proved in this and previous works (Cruz-Hernández *et al.*, 2016). These findings must be taken into consideration in AMD natural systems and the design of treatment plants in which the use of sink-phases is part of the purification system. Nevertheless, further work will be done to include the formation of more stable phases such as hematite, to evaluate the behavior of trace elements during the complete transformation of AMD precipitates.

Acknowledgements

This research was financed by the Spanish Ministry of Economy and Competitiveness through the SCYRE project (CGL2016-78783-C2-1-R). P. Cruz-Hernandez was supported by the Project FONDECYT Postdoctoral (3170082) and SCR-MAHG. M.B.J. Lindsay acknowledges support from the NSERC Discovery Grants Program (Grant No. RGPIN-2014-06589). High-energy diffraction analysis was performed at the ID22 Beamline at the European Synchrotron Radiation Facility (ESRF, Grenoble, France). Authors would like to thank the editors for their help, and Rocío Ojeda for reviews.

References

Acero, P., Ayora, C., Torrentó, C., Nieto, J.M. (2006): The behavior of trace elements during schwertmannite precipitation and subsequent transformation into goethite and jarosite. Geochim. Cosmochim. Acta, 70, 4130–4139. doi: 10.1016/j.gca.2006.06. 1367.

Adra, A., Morin, G., Ona-Nguema, G., Menguy, N., Maillot, F., Casiot, C., Bruneel, O., Lebrun, S., Juillot, F., Brest, J. (2013): Arsenic scavenging by aluminum-substituted ferrihydrites in a circumneutral pH river impacted by acid mine drainage. Environ. Sci. Technol., 47, 12784–12792. doi: 10.1021/es4020234.

Antelo, J., Fiol, S., Gondar, D., López, R., Arce, F. (2012): Comparison of arsenate, chromate and molybdate binding on schwertmannite: surface adsorption vs anion-exchange. J. Colloid Interface Sci., 386, 338–343. doi: 10.1016/j.jcis.2012.07.008.

Barham, R.J. (1997): Schwertmannite: a unique mineral, contains a replaceable ligand, transforms to jarosites, hematites, and/or basic iron sulfate. J. Mater. Res., 12, 2751–2758.

Bigham, J.M., Schwertmann, U., Carlson, L., Murad, E. (1990): A poorly crystallized oxyhydroxysulfate of iron formed by bacterial oxidation of Fe(II) in acid mine waters. Geochim. Cosmochim. Acta, 54, 2743–2758. doi: 10.1016/0016-7037(90)90009-A.

Bigham, J.M., Schwertmann, U., Traina, S.J., Winland, R.L., Wolf, M. (1996): Schwertmannite and the chemical modeling of iron in acid sulfate waters. Geochim. Cosmochim. Acta, 60, 2111–2121. doi: 10.1016/0016-7037(96)00091-9.

Bolanz, R.M., Wierzbicka-Wieczorek, M., Čaplovičová, M., Uhlík, P., Göttlicher, J., Steininger, R., Majzlan, J. (2013): Structural incorporation of As5+ into hematite. Environ. Sci. Technol., 47, 9140–9147. doi: 10.1021/es305182c.

Burton, E.D., Bush, R.T., Johnston, S.G., Watling, K.M., Hocking, R.K., Sullivan, L.A., Parker, G.K. (2009): Sorption of Arsenic(V) and Arsenic(III) to schwertmannite. Environ. Sci. Technol., 43, 9202–9207. doi: 10.1021/es902461x.

Burton, E.D., Johnston, S.G., Kraal, P., Bush, R.T., Claff, S. (2013): Sulfate availability drives divergent evolution of arsenic speciation during microbially mediated reductive transformation of schwertmannite. Environ. Sci. Technol., 47, 2221–2229. doi: 10.1021/es303867t.

Caraballo, M.A., Rimstidt, J.D., Macías, F., Nieto, J.M., Hochella, M.F. (2013): Metastability, nanocrystallinity and pseudo-solid solution effects on the understanding of schwertmannite solubility. Chem. Geol., 360–361, 22–31. doi: 10.1016/j.chemgeo.2013. 09.023.

Carlson, L., Bigham, J.M., Schwertmann, U., Kyek, A., Wagner, F. (2002): Scavenging of As from acid mine drainage by schwertmannite and ferrihydrite: a comparison with synthetic analogues. Environ. Sci. Technol., 36, 1712–1719. doi: 10.1021/ es0110271.

Carrero, S., Pérez-López, R., Fernandez-Martinez, A., Cruz-Hernández, P., Ayora, C., Poulain, A. (2015): The potential role of aluminium hydroxysulphates in the removal of contaminants in acid mine drainage. Chem. Geol., 417, 414–423. doi: 10.1016/j.chemgeo.2015.10.020.

Cruz-Hernández, P., Pérez-López, R., Parviainen, A., Lindsay, M.B.J., Nieto, J.M. (2016): Trace element-mineral associations in modern and ancient iron terraces in acid drainage environment. Catena, 147, 386–393. doi: 10.1016/j.catena.2016.07. 049.

Davidson, L.E., Shaw, S., Benning, L.G. (2008): The kinetics and mechanisms of schwertmannite transformation to goethite and hematite under alkaline conditions. Am. Mineral., 93, 1326–1337. doi: 10.2138/am.2008.2761.

Eskandarpour, A., Onyango, M.S., Ochieng, A., Asai, S. (2008): Removal of fluoride ions from aqueous solution at low pH using schwertmannite. J. Hazard. Mater., 152, 571–579. doi: 10.1016/j.jhazmat.2007.07.020.

Essalhi, M., Sizaret, S., Barbanson, L., Chen, Y., Lagroix, F., Demory, F., Nieto, J.M., Sáez, R., Capitán, M.A´ . (2011): A case study of the internal structures of gossans and weathering processes in the Iberian Pyrite Belt using magnetic fabrics and paleomagnetic dating. Miner. Deposita, 46, 981–999. doi: 10.1007/s00126-011-0361-8.

Farrow, C.L., Juhás, P, Liu, J.W., Bryndin, D., Bozin, E.S., Bloch, J., Proffen, T., Billinge, S.J.L. (2009): PDFgui user guide.

Fernandez-Martinez, A., Timon, V., Romaman-Ross, G., Cuello, G.J., Daniels, J.E., Ayora, C. (2010): The structure of schwertmannite, a nanocrystalline iron oxyhydroxysulfate. Am. Mineral., 95, 1312–1322. doi: 10.2138/am.2010.3446.

Fukushi, K., Sasaki, M., Sato, T., Yanase, N., Amano, H., Ikeda, H. (2003a): A natural attenuation of arsenic in drainage from an abandoned arsenic mine dump. Appl. Geochem., 18, 1267–1278. doi: 10.1016/S0883-2927(03)00011-8.

Fukushi, K., Sato, T., Yanase, N. (2003b): Solid-solution reactions in As(V) sorption by schwertmannite. Environ. Sci. Technol., 37, 3581–3586. doi: 10.1021/es026427i.

Gagliano, W.B., Brill, M.R., Bigham, J.M., Jones, F.S., Traina, S.J. (2004): Chemistry and mineralogy of ochreous sediments in a constructed mine drainage wetland. Geochim. Cosmochim. Acta, 68, 2119–2128. doi: 10.1016/j.gca.2003.10.038.

Harrington, R., Hausner, D.B., Bhandari, N., Strongin, D.R., Chapman, K.W., Chupas, P.J., Middlemiss, D.S., Grey, C.P., Parise, J.B. (2010): Investigation of surface structures by powder diffraction: a differential pair distribution function study on arsenate sorption on ferrihydrite. Inorg. Chem., 49, 325–330. doi: 10.1021/ic9022695.

Juhás, P., Davis, T., Farrow, C.L., Billinge, S.J.L. (2013): PDFgetX3: a rapid and highly automatable program for processing powder diffraction data into total scattering pair distribution functions. J. Appl. Crystallogr., 46, 560–566.

Kieffer, J., Karkoulis, D. (2013): PyFAI, a versatile library for azimuthal regrouping. J. Phys. Conf. Ser., 425, 20212. doi: 10.1088/1742-6596/425/20/202012.

Krause, E. & Ettel, V.A. (1989): Solubilities and stabilities of ferric arsenate compounds. Hydrometallurgy, 22, 311–337. doi: 10.1016/0304-386X(89)90028-5.

Li, W., Harrington, R., Tang, Y., Kubicki, J.D., Aryanpour, M., Reeder, R.J., Parise, J.B., Phillips, B.L. (2011): Differential pair distribution function study of the structure of arsenate adsorbed on nanocrystalline c-alumina. Environ. Sci. Technol., 45, 9687–9692. doi: 10.1021/es200750b.

Lindsay, M.B.J., Moncur, M.C., Bain, J.G., Jambor, J.L., Ptacek, C.J., Blowes, D.W. (2015): Geochemical and mineralogical aspects of sulfide mine tailings. Appl. Geochem., 57, 157–177. doi: 10.1016/j.apgeochem.2015.01.009.

Loan, M., Cowley, J.M., Hart, R., Parkinson, G.M. (2004): Evidence on the structure of synthetic schwertmannite. Am. Mineral., 89, 1735–1742.

Maillot, F., Morin, G., Juillot, F., Bruneel, O., Casiot, C., Ona-Nguema, G., Wang, Y., Lebrun, S., Aubry, E., Vlaic, G., Brown, G.E. (2013): Structure and reactivity of As(III)- and As(V)-rich schwertmannites and amorphous ferric arsenate sulfate from the Carnoule`s acid mine drainage, France: comparison with biotic and abiotic model compounds and implications for As remediation. Geochim. Cosmochim. Acta, 104, 310–329. doi: 10.1016/j.gca.2012.11.016.

Mandal, B.K. & Suzuki, K.T. (2002): Arsenic round the world: a review. Talanta, 58, 201–235. doi: 10.1016/S0039- 9140(02)00268-0.

Nieto, J.M., Sarmiento, A.M., Canovas, C.R., Olias, M., Ayora, C. (2013): Acid mine drainage in the Iberian Pyrite Belt: 1. Hydrochemical characteristics and pollutant load of the Tinto and Odiel rivers. Environ. Sci. Pollut. Res., 20, 7509–7519. doi: 10.1007/s11356-013-1634-9.

Nordstrom, D.K. & Alpers, C.N. (1999): Geochemistry of acid mine waters, Society of Economic Geologists, Littleton.

Nordstrom, D.K., Wilde, F.D. (1998): Reduction-oxidation potential (electrode method). in National Field Manual for the Collection of Water Quality Data. US Geological Survey, Reston, VA. Book 9, ch. 6.5. US Geological Survey techniques of water resources investigations. 20 p.

Paktunc, D., Dutrizac, J., Gertsman, V. (2008): Synthesis and phase transformations involving scorodite, ferric arsenate and arsenical ferrihydrite: implications for arsenic mobility. Geochim. Cosmochim. Acta, 72, 2649–2672. doi: 10.1016/j.gca.2008.03.012.

Park, J.H., Han, Y.S., Ahn, J.S. (2016): Comparison of arsenic co-precipitation and adsorption by iron minerals and the mechanism of arsenic natural attenuation in a mine stream. Water Res., 106, 295–303. doi: 10.1016/j.watres.2016.10.006.

Parviainen, A., Cruz-Hernández, P., Pérez-López, R., Nieto, J.M., Delgado-López, J.M. (2015): Raman identification of Fe precipitates and evaluation of As fate during phase transformation in Tinto and Odiel River Basins. Chem. Geol., 398, 22–31. doi: 10.1016/j.chemgeo.2015.01.022.

Parviainen, A., Lindsay, M.B.J., Pérez-López, R., Gibson, B.D., Ptacek, C.J., Blowes, D.W., Loukola-Ruskeeniemi, K. (2012): Arsenic attenuation in tailings at a former Cu-W-As mine, SW Finland. Appl. Geochem., 27, 2289–2299. doi: 10.1016/ j.apgeochem.2012.07.022.

Pérez-López, R., Asta, M.P., Román-Ross, G., Nieto, J.M., Ayora, C., Tucoulou, R. (2011): Synchrotron-based X-ray study of iron oxide transformations in terraces from the Tinto-Odiel river system: influence on arsenic mobility. Chem. Geol., 280, 336–343. doi: 10.1016/j.chemgeo.2010.11.021.

Regenspurg, S. & Peiffer, S. (2005): Arsenate and chromate incorporation in schwertmannite. Appl. Geochem., 20, 1226–1239. doi: 10.1016/j.apgeochem.2004.12.002.

Schwertmann, U. & Cornell, R.M. (1991): Iron oxides in the laboratory, Wiley, New York.

Schwertmann, U. & Fitzpatrick, R.W. (1992): Iron minerals in surface environments. Catena Suppl., 21, 7–30.

Takeshi, E. & Billinge, S.J.L. (2012): Concluding remarks. Pergamon Mater. Series, 16, 467–469. doi: 10.1016/B978-0- 08-097133-9.00013-7.

Wang, X., Gu, C., Feng, X., Zhu, M. (2015): Sulfate local coordination environment in schwertmannite. Environ. Sci. Technol., 49, 10440–10448. doi: 10.1021/acs.est.5b02660.

Yu, J.Y., Heo, B., Choi, I.K., Cho, J.P., Chang, H.W. (1999): Apparent solubilities of schwertmannite and ferrihydrite in natural stream waters polluted by mine drainage. Geochim. Cosmochim. Acta, 63, 3407–3416. doi: 10.1016/S0016- 7037(99)00261-6.

Supplementary Material

- pdf file